Paper

Simulation of Scattering from Complex Rough Surfaces at Low Grazing Angle Incidence Using the GFBM/SAA Method

Ya-Qiu Jin [1,2] and Zhongxin Li [2]
1 on leave at Department of Electronic Engineering
City University of Hong Kong, Hong Kong SAR, China
2 Center for Wave Scattering and Remote Sensing
Fudan University, Shanghai 200433, China

A comprehensive approach of combining the generalized forward-backward method (GFBM) with spectral accelerate algorithm (SAA) is developed. It is applied to numerical simulation of bistatic scattering from two models: (1) an ocean-like surface described by the Pierson-Moskowitz spectrum with a ship presence, and (2) a fractal rough surface described by the Weierstrass-Manderbrot function under the TE and TM tapered wave incidence at low grazing angle (LGA). Numerical simulations of bistatic scattering at LGA show the functional dependence upon polarization, frequency, observation angle and other surface parameters.

Keywords: scattering simulation, rough surface with target, GFBM/SAA

1. Introduction

Scattering from rough surface in low grazing angle (LGA) has attracted much attention due to practical importance in the areas of the low-attitude/long-range radar surveillance, target tracking, communication, and navigation systems operating at low grazing conditions above the ocean surface. Conventional analytic theories of scattering from rough surface derived from some approximations, such as the Kirchhoff and small perturbation approximations, two-scale method, or integral equation method etc., are not able to take into account for multiple scattering and multi-path propagation, wedge diffraction and shadowing, etc. at the LGA conditions. There are fundamental changes in the characteristics of the sea clutter as LGA incidence approaches. Sea spikes associated with the unstable sharp-crested or breaking wave occur and, especially, enhance the co-horizontally polarized (*hh*) echo signal. It also causes dislocation of the Doppler spectra peaks [1].

In recent years, numerical methods, such as the method of moment (MoM) and finite elements method with Monte Carlo realizations have been developed for study of scattering from rough surface[2,3]. However, as LGA approaches, computation might become very intensive to require long surface and large number of surface unknowns.

Several different methods have been developed in recent years in order to reduce the number of computer operations. A forward-backward method (FBM) [4,5] has been developed for solving the magnetic field integral equation (MFIE). This method splits the surface current at each point into two components. One is the forward contribution due to the incident field and the radiation of the current elements located in front of the receiving element, and another is the backward contribution due to the current elements located beyond the receiving element. The forward component is first found over the whole surface and then is used to determine the backward contribution. This procedure is repeated iteratively until a converged solution is reached. The operational counts are $O(N^2)$ (of the order N^2, N is the unknowns). To further speed up the FBM calculation, a spectral accelerate algorithm (SAA) of the Green's function was studied [6,7]. The computational cost and storage requirements can be reduced to $O(N)$.

However, these methods remained to be further studied for scattering from composite surface with a target presence or breaking wave on rough surface. A geometric picture is illustrated in Fig.1.

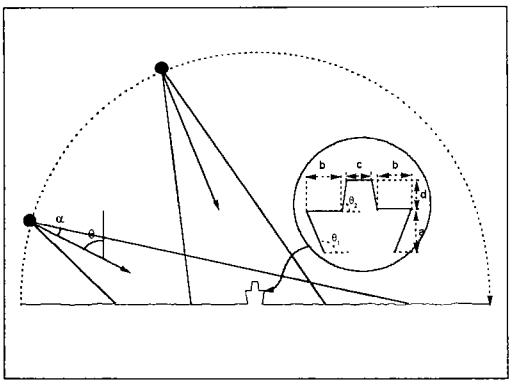

Fig.1 Geometry of the problem

A generalized forward-backward method (GFBM) has been recently developed in Ref. (8). The GFBM combines conventional FBM with the MoM, and applies the MoM especially to the target region containing nearby sea surface. The solution is iteratively obtained based on the FBM process. The computational cost of the GFBM is similar to

the FBM, since it only includes additional cost associated with the direct MoM for a small target region. However, the GFBM of Ref.(8) has been discussed only for a few TE case without SAA. The lit region of the surface was simply taken to be finite and thus decreased the accuracy of computed scattered fields.

As another model of rough surface, the fractal geometry was introduced during recent years. Since fractal geometry holds in balance long-range order and short-range disorder and can be used to describe both deterministic and random structures, it seems better to describe some natural surfaces. The fractal geometry serves as a bridge between periodic function and random function. The fractal model has also been introduced to study of scattering from sea surface [9].

In this paper, a comprehensive method of the GFBM with SAA is developed. The tapered incident wave is employed to obtaining a finite lit surface [10]. It is applied to numerical simulations of bistatic scattering from two models: (1) one-dimensional (1-D) rough ocean-like surface with a ship presence, and (2) a complex fractal rough surface under the TE (horizontally polarized, *h*) or TM (vertically polarized, *v*) incidences at LGA.

2. The FBM and GFBM for EFIE and MFIE

A tapered wave, $E^{inc}(x,z)$ or $H^{inc}(x,z)$, is incident upon a 1-D dielectric rough surface S', the electric field integral equation (EFIE) and magnetic field integral equation (MFIE) are written respectively as

$$\frac{E_y(r)}{2}\delta(r-r') = E_y^{inc}(r) + \int_{S'}[E_y(r')\frac{\partial G(r,r')}{\partial n'} - G(r,r')\frac{\partial E_y(r')}{\partial n'}]dS' \quad (1)$$

$$\frac{H_y(r)}{2}\delta(r-r') = H_y^{inc}(r) + \int_{S'}[H_y(r')\frac{\partial G(r,r')}{\partial n'} - G(r,r')\frac{\partial H_y(r')}{\partial n'}]dS' \quad (2)$$

The random surface height has $z = f(x)$ and $< f(x) >= 0$.

Making use of the MoM formulation with a set of N pulse-basis functions and point-matching weighting at center of each current element [11], Eqs. (1,2) are discretized to form the matrix equation

$$\overline{\overline{Z}} \cdot \bar{I} = \bar{V} \quad (3)$$

where $\overline{\overline{Z}}$ is impedance matrix, $\bar{V}$ is incidence vector, $\bar{I}$ is induced current along the rough surface. The formulations of all terms in Eq. (3) can be referred to Refs. (6-8).

In the FBM, the matrices of Eq. (3) are decomposed as

$$\bar{I} = \bar{I}_f + \bar{I}_b \quad (4)$$

$$\overline{\overline{Z}} = \overline{\overline{Z}}_f + \overline{\overline{Z}}_s + \overline{\overline{Z}}_b \quad (5)$$

where $\bar{I}_f$ is the forward component (i.e. the current contribution due to the waves propagating in the forward direction), $\bar{I}_b$ is the backward component (i.e. current contribution due to the waves propagating in the backward direction). And $\overline{\overline{Z}}_f$, $\overline{\overline{Z}}_s$ and $\overline{\overline{Z}}_b$ are, respectively, the lower triangular part, self-impedance term, and upper triangular part of $\overline{\overline{Z}}$.

Substituting Eqs. (4,5) into Eq. (3), it can now be separated into two forward- and backward-equations as follows,

$$\overline{\overline{Z}}_s \cdot \bar{I}_f = \bar{V} - \overline{\overline{Z}}_b \cdot (\bar{I}_f + \bar{I}_b) \quad (6)$$

$$\overline{\overline{Z}}_s \cdot \bar{I}_b = -\overline{\overline{Z}}_b \cdot (\bar{I}_f + \bar{I}_b) \quad (7)$$

Eqs. (6,7) can be solved, iteratively, with starting $\bar{I}_b^{(0)} = 0$. Convergence has been extremely fast for moderately rough surfaces, e. g. less than six iterations,

However, the FBM algorithm might become unstable for re-entrant surfaces, e.g. due to the ship presence in Fig.1. The GFBM is needed especially to take into account for scattering from the ship region.

The difference between the GFBM and FBM is decomposition of the matrix $\overline{\overline{Z}}$ as

$$\overline{\overline{Z}} = \overline{\overline{Z}}_{fg} + \overline{\overline{Z}}_{sg} + \overline{\overline{Z}}_{bg} \quad (8)$$

where $\overline{\overline{Z}}_{sg}$ is the diagonal part of $\overline{\overline{Z}}$ with an additional block to include the sub-matrix due to ship target and nearby sea surface; $\overline{\overline{Z}}_{fg}$ and $\overline{\overline{Z}}_{bg}$ are, respectively, the lower-triangular and upper-triangular parts of $\overline{\overline{Z}}$, excluding the part of $\overline{\overline{Z}}_{sg}$. Using this decomposition, the matrix $\overline{\overline{Z}}_{sg}$ contains both the self (diagonal) term and the interaction of the target and nearby sea surface.

Substituting Eqs.(4,6) into (3), it yields the following matrix equations:

$$\overline{\overline{Z}}_{sg} \cdot \bar{I}_f = \bar{V} - \overline{\overline{Z}}_{fg} \cdot (\bar{I}_f + \bar{I}_b) \quad (9)$$

$$\overline{\overline{Z}}_{sg} \cdot \bar{I}_b = -\overline{\overline{Z}}_{bg} \cdot (\bar{I}_f + \bar{I}_b) \quad (10)$$

Above equations are iteratively solved for $(\bar{I}_f^{(i)}, \bar{I}_b^{(i)})$ from

$$(\overline{\overline{Z}}_{sg} + \overline{\overline{Z}}_{fg}) \cdot \bar{I}_f^{(i)} = \bar{V} - \overline{\overline{Z}}_{fg} \cdot \bar{I}_b^{(i-1)} \quad (11)$$

$$(\overline{\overline{Z}}_{sg} + \overline{\overline{Z}}_{bg}) \cdot \bar{I}_b^{(i)} = -\overline{\overline{Z}}_{bg} \cdot \bar{I}_f^{(i)} \quad (12)$$

with starting $\bar{I}_b^{(0)} = 0$.

Computational cost of the GFBM is practically the same as the conventional FBM, but with the additional MoM computation of factorizing $\overline{\overline{Z}}_{sg}$. Due to the limited size of this block, its factorization can be performed once and stored for next iterations. Thus, the GFBM has computational cost of $O(N^2)$ per iteration as the FBM. The storage requirement is $O(N)$ to store the iterated currents with additional $M \times M$ matrix storage. Generally, it always has $M << N$. It is noted that the full $\overline{\overline{Z}}$ matrix is not stored, so it is necessary to re-compute the matrix elements in each iteration (except for the inner MoM matrix associated with the target region).

3. The Spectral Accelerate Algorithm (SAA)

It can be seen from Eqs.(1,2 or 3) that iterative procedures repeat computation of Green's function of Eqs.(1,2) or $\overline{\overline{Z}}^f \cdot \bar{I}$ and $\overline{\overline{Z}}^b \cdot \bar{I}$ in Eq.(3), i.e.

$$V_f(r_n)=\sum_{m=1}^{n-1}Z_{nm}^f I_m \quad \text{and} \quad V_b(r_n)=\sum_{m=n+1}^{N}Z_{nm}^b I_m \tag{13}$$

It requires $O(N^2)$ operations. Define the neighborhood distance L_s and classify the interactions between the points within L_s as strong and those outside of L_s as weak. Thus, Eq. (13) is rewritten as

$$V_f(r_n)=V_s+V_w=\sum_{m=n-N_s-1}^{n-1}Z_{nm}^f I_m+\sum_{m=1}^{n-N_s-1}Z_{nm}^f I_m \tag{14}$$

V_b of Eq. (13) can also be treated in the same fashion. The strong V_s is found in conventional manner using the exact matrix elements. The weak V_w radiated from the sources outside the strong sources becomes important when the incidence angle approaches to the grazing or if one is interested in back-scattered field. Computation of V_w takes most CPU time consuming via the exact computation. It makes FBM very inefficient. Substituting the spectral representation of the Green function [12] into Eqs. (1-3), it is derived that

$$V_w(r_n)=\sum_{m=1}^{n-N_s-1}Z_{nm}^f I_m=\frac{i\Delta x}{4\pi}\int_{C_\theta}F_n(\theta)\exp(ikz_n\sin\theta)d\theta \tag{15}$$

where for TE incidence

$$\begin{aligned}F_n(\theta)&=F_{n-1}(\theta)e^{ik\Delta x\cos\theta}\\&+I_{n-N_s-1}\left[\frac{1}{\sqrt{\varepsilon_1}}(-\sin\theta+f_{x_n}\cos\theta)+\sqrt{1+f_{x_m}^2}\right]\\&\times\exp[ik(N_s+1)\Delta x\cos\theta]\exp(-ikz_{n-N_s-1})\sin\theta\end{aligned} \tag{16a}$$

for TM incidence:

$$\begin{aligned}F_n(\theta)&=F_{n-1}(\theta)e^{ik\Delta x\cos\theta}\\&+I_{n-N_s-1}\cdot\left[ik(-\sin\theta+f_{x_n}\cos\theta)+\frac{1}{\sqrt{\varepsilon_1}}\sqrt{1+f_x^2}\right]\\&\times\exp[ik(N_s+1)\Delta x\cos\theta]\exp(-ikz_{n-N_s-1})\sin\theta\end{aligned} \tag{16b}$$

It can be seen from Eqs. (15,16) that $F_n(\theta)$ can be easily found by recursive procedure without much computation.

All above SAA equations can be degenerated into the one for perfectly conducting surface when $\varepsilon_1\to\infty$.

It is desired to employ a new integration contour C_δ instead of C_θ, in Eq. (15), because the far field pattern of $F_n(\theta)$ in real θ space tends to have a narrow main lobe and many side lobes for a large surface in contrast to a slowly varying pattern along C_δ, as discussed in Refs. (6,7).

4. Numerical Simulations

The GFBM/SAA is applied to numerical simulations of bistatic scattering from ocean-like randomly rough, perfectly conducting surface. The rough sea surface is described by the 1-D Pierson-Moskowitz (P-M) spectrum proposed by Thorsos [14],

$$W(K)=\frac{A}{4|K|^3}e^{-Bg_0^2/(K^2U^4)} \tag{17}$$

where K is the spatial wave-number, U *(m/s)* is the wind speed defined at *19.5 m* above the sea surface, the gravity acceleration $g_0=9.81\ m/s^2$, and the empirical coefficients $A=8.10\times10^{-3}$, $B=0.74$.

The band-limited Weierstrass-Manderbrot function [14] is employed to describe the fractal rough surface as

$$f(x)=\delta\cdot C\sum_{n=0}^{N-1}b^{(D-2)n}\sin(k_0b^nx+\varphi_n) \tag{18}$$

where D $(1<D<2)$ is the fractal dimension, φ_n is random phase, $b(>1)$ the spatial frequency scaling parameter, k_0 the fundamental spatial wave number, and δ the rms surface height. The normalized amplifier control parameter is $C=\sqrt{2(1-b^{2(D-2)})/(1-b^{2N(D-2)})}$.

As Eq. (18) indicated, the fractal surface is described by the parameters δ, D, b, k_0 and N, whilst the conventional Gaussian surface only needs two parameters, δ and ℓ. Different fractal rough surfaces may have the same δ and ℓ. Fractal rough surface is multi-scales rough surface whilst the Gaussian rough surface is a single scale rough surface.

Surface realizations are generated using the Monte Carlo method with the FFT similar to that described in Ref.(13). Fifty realizations are generated in this paper to implement average calculation through the Monte Carlo method.

The bistatic scattering coefficient for TE tapered incidence is defined [15,16] as

$$\sigma_{TE}^{(U)}(\theta_{in},\theta_s)=\frac{\left|\int_{S'}\left[\frac{ik(f_{x'}\sin\theta_s-\cos\theta_s)}{\sqrt{1+f_{x'}^2}}E-\frac{\partial E}{\partial n'}\right]e^{-ik(x'\sin\theta_s+z'\cos\theta_s)}dS'\right|^2}{8\pi k\sqrt{\frac{\pi}{2}}g\cos\theta_{in}\left(1-\frac{1+2\tan^2\theta_{in}}{2(kg)^2}\right)} \tag{19}$$

where the superscript U indicates scattering to the upper-half space, and subscript TE denotes the TE incidence. The parameter g is the tapered scale to govern the tapered width and usually is taken as $L/6$.

For $\sigma_{TM}^{(U)}$ of the TM incidence, the electric field E in Eq. (21) is replaced by magnetic fields H.

And for calculations of transmitting coefficients $\sigma_{TE}^{(D)}$ and $\sigma_{TM}^{(D)}$ through the surface (superscript D denotes down-going into lower-half space), the terms with $k, \partial/\partial n'$ of the upper half-space should be replaced by $k_1, \partial/\partial n_1'$ of the lower half-space.

The wavelength of incident wave is taken as $\lambda=1m$, the illuminated surface length $L=409.6\lambda$ and $g=L/6$. The geometric size of the ship target is supposed as $a=9m$, $b=5m$, $c=4m$, $d=6m$, $\theta_1=100^o$, $\theta_2=80^o$ as described in Fig.1. The ship on the illuminated rough surface is located at 348.16λ in following examples.

The code of GFBM/SAA is first testified to compare with the MoM result for one surface realization. Two results are almost exactly matched. The GFBM/SAA needs 16 *min* (TE)

and 8 *min* (TM) for calculations, but the MoM took 2 *hrs* for both TE and TM cases. The computations are carried out in the Pentiam II PC.

The GFBM/SAA is also compared with GFBM without SAA. It shows that GFBM/SAA is twice faster than GFBM.

Furthermore, the energy conservation from calculations of reflectivity R and transmittivity T, by integrating bistatic scattering over the upper- and down- (for the dielectric case) half space, yields the accuracy estimation of the GFBM/SAA as the proof of $R+T=1$.

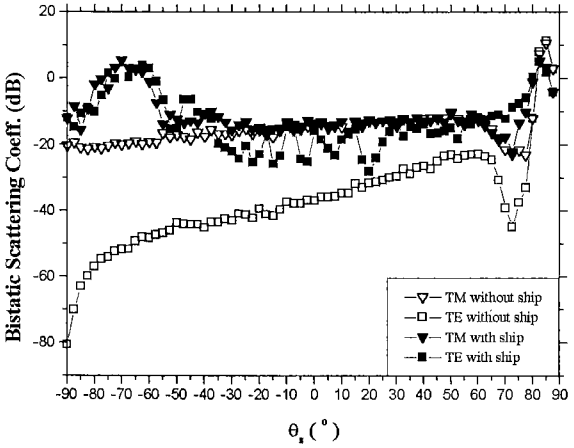

Fig.2 Bistatic scattering vs observation angle

Fig.2 presents the bistatic scattering at θ_s from the conducting sea surface at $U= 3\ m/s$ for TE and TM incidence at LGA $\theta_{inc} = 85°$, respectively. The no-filled lines denote the scattering from sea surface without ship, and the filled lines denote scattering from sea surface with a ship presence. In the case without ship, backscattering $\sigma_{hh} << \sigma_{vv}$ (here *hh* and *vv* indicate co-polarized hh and vv for the TE (h) and TM (v) cases, respectively), and scattering in forward direction is dominant. But in the case with a ship presence, bistatic scattering, especially in backward direction, is significantly increased, and it might yield backscattering $\sigma_{hh} > \sigma_{vv}$. This is a characteristic of scattering from spatially inhomogeneous sea surface at LGA.

It can be seen that induced current over the ship target is extremely increased, and the induced current for TE incidence is stronger than the case of TM incidence. It is a reason for $\sigma_{hh} > \sigma_{vv}$.

Forward scattering is dominant at low wind speed and without ship presence. As the sea wind speed increases, the surface becomes much rougher to yield more diffused scattering. As the ship is placed over the sea surface, significant changes of bistatic scattering happen in the forward and backward directions and backscattering is extremely enhanced, especially σ_{hh}.

Comparing the no-filled lines indicated by 'cond' and 'diel' respectively for the models of perfect conducting and dielectric media, it can be seen that the model difference is negligible for TE case, but not for TM case.

Fig.3 presents back-scattering coefficients vs. incident angle at $U=3\ m/s$. It can be seen that the ship presence significantly changes scattering pattern at low grazing angle (large incident angle).

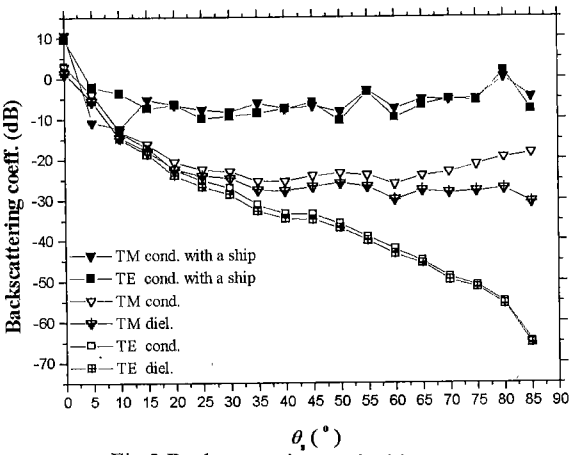

Fig.3 Back-scattering vs. incident angle

Let's turn to the fractal model. The surface is simply taken as perfectly conducting. Figs. 4 and 5 show the TE bistatic scattering from three fractal surfaces ($D=1.1, 1.6, 1.9$ and $\delta = 0.05\lambda$) at incident angles $30°$ and $80°$, respectively.

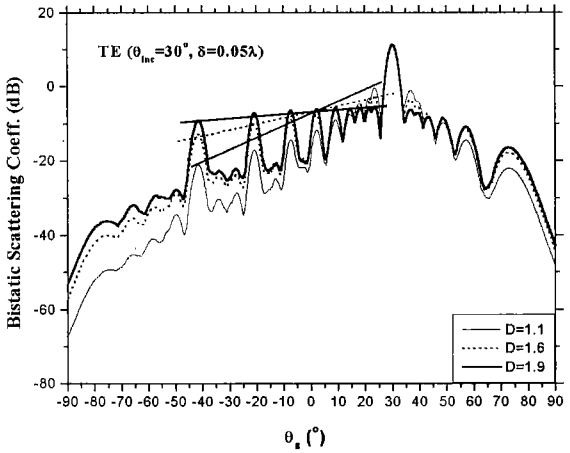

Fig.4 Bistatic scattering from fractal surfaces

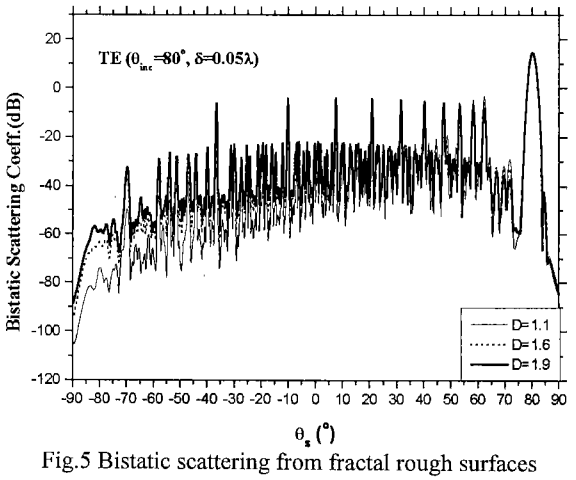

Fig.5 Bistatic scattering from fractal rough surfaces

It is interesting to see that in either TE or TM cases angular scattering pattern shows significant oscillation, and the line to link the crests along both sides of the specular reflection are linearly related with D.

As δ becomes larger, much rough surface yields diffused scattering and linear slope is not well identified.

Fig.6 shows bistatic scattering as an artificial triangular object (width 2λ, height λ) is placed over the fractal surface.

It can be seen that angular oscillation is darken due to the object presence.

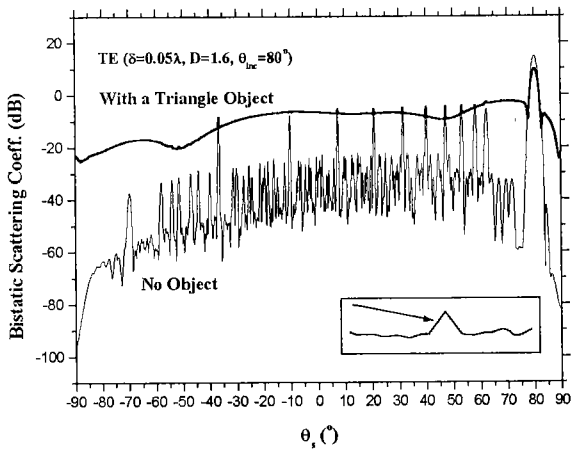

Fig.6 Bistatic scattering from complex fractal surface

5. Conclusions

A comprehensive GFBM/SAA is developed for numerical simulation of bistatic scattering from a 1-D sea surface realized by the P-M spectrum or fractal rough surfaces. Bistatic scattering from ocean-like surface with a ship presence or fractal surface for TE and TM incidence at LGA are calculated. Its functional dependence upon physical parameters such as polarization, scattering angle, wind speed, etc. are simulated. Its efficiency is validated by the energy conservation and is compared with MoM and other methods. It can be seen that

(1) Bistatic scattering from sea surface with a ship presence shows significant angular variation, especially for TE incidence. Especially, backward scattering is enhanced.

(2) Without ship presence it generally has $\sigma_{hh} << \sigma_{vv}$. But the presence of a ship might cause $\sigma_{hh} > \sigma_{vv}$.

(3) Modeling difference between the perfectly conducting and dielectric sea surfaces is negligible for TE case, but not for TM case.

(4) Bistatic scattering from fractal surface shows strong angular oscillation, and the line slope to link the crests is linearly related with fractal parameter.

(Manuscript received December 25, 2000, revised May 7, 2001)

Acknowledgment

This work was supported by the grant No.49831060 of the China National Science Foundation. Jin is also grateful to City University of Hong Kong for support of the academic visit.

References

(1) G. S. Brown, Special issue on low-grazing-angle backscattering from rough surface, *IEEE Transactions on Antennas Propagation*, **46**, 2028 (1998).

(2) Y. Q. Jin, G. Li, Detection of a scatter target over randomly rough surface by using angular correlation function in finite element approach, *Waves in Random Media*, **10**, 273 (2000).

(3) S. H. Lou, L. Tsang, C. H. Chan and A. Ishimaru, Application of the finite element method to Monte Carlo simulations of scattering of waves by random rough surfaces with the periodic boundary condition, *Journal of Electromagnetic Waves and Applications*, **5**, 835 (1991).

(4) D. Holliday, L. L. DeRaad, and G. J. St-Cyr, Forward-backward: A new method for computing low-grazing angle scattering, *IEEE Transactions on Antennas Propagation*, **44**, 722 (1996).

(5) D. Holliday, L. L. DeRaad, and G. J. St-Cyr, Forward-backward method for scattering from imperfect conductors, *IEEE Transactions on Antennas Propagation*, **46**, 101 (1998).

(6) H. T. Chou, J. T. Johnson, A novel acceleration algorithm for the computation of scattering, from rough surfaces with the forward-backwards method, *Radio Science*, **33**, 1277 (1998).

(7) H. T. Chou, J. T. Johnson, Formulation of forward-backward method using novel spectral acceleration for the modeling of scattering from impedance rough surfaces, *IEEE Transactions on Geosicence and Remote Sensing*, **38**, 605 (2000).

(8) M. R. Pino, L. Landesa, J. L. Rodriguez, etc., The generalized Forward-Backward method for analyzing the scattering from targets on ocean-like rough surfaces, *IEEE Transactions on Antennas and Propagation*, **47**, 961 (1999).

(9) F. Berizzi and E. Dalle-Mese, Fractal analysis of the signal scattering from the sea surface, *IEEE transactions on antenna propagation*, **47**, 324 (1999).

(10) K.F. Warnic and W.C. Chew, Numerical simulation methods for rough surface scattering, *Waves in Random Media*, **11**, R1 (2001).

(11) R.F. Harrington, *Field Computation by Moment Method*, New York, IEEE Press, (1993).

(12) J. A. Kong, *Electromagnetic Wave Theory*, New York, Wiley (1985).

(13) E. Thorsos, Acoustic scattering from 'Pierson-Moskowitz' sea surface, *Journal of the Acoustic Society of the America*, **88**, 335 (1998).

(14) S. Savailis et al., Scattering from fractally corrugated surfaces with tuse of the extended boundary condition method, *J. Opt. Soc. Am*, **14**, 475 (1997).

(15) Q. Li, C. H. Chan, and T. Tsang, Monte Carlo simulations of wave scattering from lossy dielectric random surfaces using the Physics-Based Two-Grid method and the Canonical-Grid method, *IEEE Transactions on Antennas Propagation*, **47**, 752 (1999).

(16) R. F. Harrington. *Field Computation by Moment Method*, New York: IEEE Press (1993).

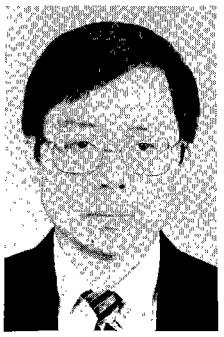

Ya-Qiu Jin graduated from Peking University in 1970, and received the M.S. (1982), E.E. (1983), and Ph.D. (1985) degrees from the Massachusetts Institute of Technology, USA. He is now a Professor of the School of Information Science and Engineering, and Director of CWSRS, Fudan University, Shanghai. He held the UK Royal Society Fellowship in 1993, the Senior Research Associateship awarded by the USA National Research Council in 1996, and Visiting Professor in City University of Hong Kong in 2001. He is Chairman of IEEE GRSS Beijing Chapter and CIE Fellow. His main interests are EM wave scattering, propagation and radiative transfer theory in random media, quantitative microwave remote sensing, and computational EM. He has published over 280 papers and five books in China and abroad. He has received the National Science Prize in 1993 among other award.

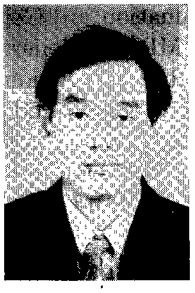

Zhongxin Li received the B.E. (1989), M.E. (1994) degrees from the Xi'an Jiaotong University, and Ph.D. (1999) degree from Tsinghua University. He is now a post-doctoral fellow at Center of Wave Scattering and Remote Sensing (CWSRS), Fudan University, Shanghai. He has published over 30 papers in China and abroad. His main interests are EM theory and its application, computational electromagnetics, and remote sensing.